14th International Symposium on Turbulence and Shear Flow Phenomena (TSFP14)
Heidelberg, Germany, July 28–31, 2026

SPATIO-TEMPORAL ENERGY SPECTRA OF DROPS IN TURBULENCE

Ianto Cannon
ZARM
University of Bremen
Bremen, Germany
ianto.cannon@zarm.uni-bremen.de

Daniel Morón and Marc Avila
ZARM
University of Bremen
Bremen, Germany

Alberto Vela-Martín
Department of Aerospace Engineering
Universidad Carlos III de Madrid
Madrid, Spain

1 ABSTRACT

We present spatio-temporal energy spectra of drops in homogeneous isotropic turbulence, computed from an ensemble of hundreds of direct numerical simulations of the Cahn–Hilliard–Navier–Stokes equations across Weber numbers We $\in \{0.73, 1.82, 2.91, 3.64\}$. Simulations are analysed during the stage of dynamic equilibrium between the drop and the surrounding turbulence, before breakup occurs. We compute spatio-temporal spectra of the turbulent kinetic energy, the interfacial force exerted on the fluid, and the interfacial area of the drops. The force spectrum confirms that drops act as a spectral shortcut: absorbing kinetic energy from large, slow eddies and returning it to small, fast eddies, with a crossover near the drop diameter and inertial timescale. The interfacial area spectrum reveals that deformation energy is concentrated at the drop-diameter length scale and at slow oscillation frequencies.

2 INTRODUCTION

Spatial energy spectra allow us to test the predictions of Kolmogorov [1], particularly in multiphase flows when additional forces act on the fluid. Recently, in particle-laden [2], and drop-laden [3, 4, 5] flows, the additional fluid phase acts as a “spectral shortcut”, removing kinetic energy from the fluid at large scales, and returning it to the flow at smaller scales. Such multiphase turbulent studies have so far been limited to spatial analysis. However, in the case of drops, the interface deforms and moves with the flow, hence a large part of the underlying physics is kept in the temporal part.

Spatio-temporal energy spectra have been used with great success to characterise wave dynamics on nearly flat interfaces, such as the ocean surface [6, 7]. More recently, spatial and temporal spectra in non-Newtonian turbulent flows have been used to compare scaling exponents in time and space [8]. To our knowledge, no spatiotemporal analysis has yet been performed for deformable drops embedded in turbulent flows.

Cannon et al. [9] showed that high strain events precede breakup in turbulent flows, and that the drops follow three distinct stages of evolution: 1-initial deformation, 2-dynamic equilibrium, and 3-breakup. Here, we present a spatio-temporal analysis of the fluid and interfacial energy of drops in stage 2-dynamic equilibrium with the surrounding turbulent flow. Energy exchanges between the fluid and the interface. The fluid stores kinetic energy, and the interface stores surface potential energy. The energy transfer can be positive or negative at a given moment in time and location on the interface; however, the net exchange is zero when averaged over the interface over the duration of stage 2.

In this work, we use direct numerical simulations of the Cahn–Hilliard–Navier–Stokes equations to build a time-resolved database of drop–turbulence interactions across a range of Weber numbers. We quantify the spatio-temporal energy spectra of the turbulent kinetic energy field, the interfacial force on the fluid, and the interfacial area of the drops. The objectives are threefold:

1. How does the turbulent kinetic energy spectrum $E(\kappa,\omega)$ deviate from classical single-phase Kolmogorov scaling in the presence of deformable drops, and how does this deviation depend on Weber number, particularly in the high-κ, high-ω regime?
2. In what way do drops redistribute energy across scales in the joint wavenumber–frequency space, as captured by the interfacial forcing spectrum $F(\kappa,\omega)$, and does this reveal a scale-dependent transfer mechanism between large, slow motions and small, fast motions across the crossover set by the drop diameter and its inertial timescale?
3. How do interfacial deformations evolve in spatio-temporal spectral space, and to what extent are the observed structures in $A(\kappa,\omega)$ governed by advective transport by the surrounding turbulence, as indicated by alignment with the scaling $\omega \sim u'\kappa$?

3 METHODOLOGY

Table 1. Parameters for different cases: Weber number We, and number of simulations N.

We	0.73	1.82	2.91	3.64	∞
N	40	104	28	7	1

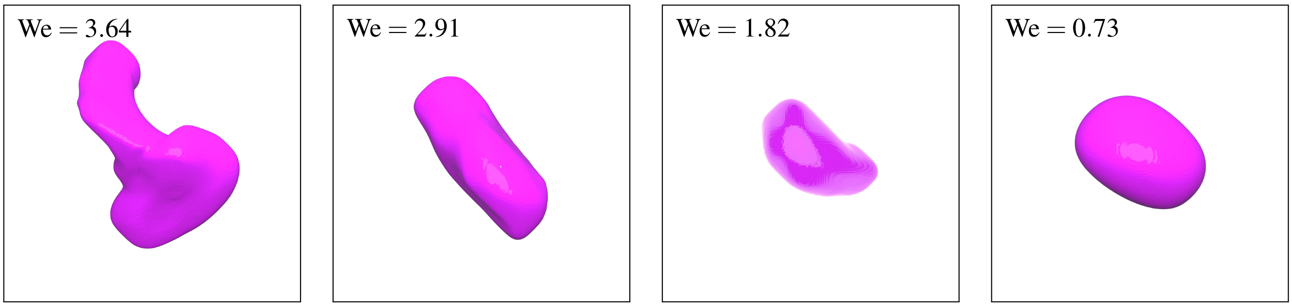

Figure 1. Snapshots of drops at each Weber number studied in these proceedings. The black border shows the simulation domain, which has side length L.

We perform direct numerical simulations of the Cahn–Hilliard–Navier–Stokes equations in homogeneous isotropic turbulence, discretised onto a triperiodic cubic grid of size $M = 256$. The Cahn–Hilliard equations are particularly suited for the spectral analysis that we carry out in this manuscript, as (unlike other multiphase methods such as the volume-of-fluid [10] or front-tracking [11]) the interfacial energy is built into the free energy functional.

We solve the Navier–Stokes equations in a triperiodic domain of size L, describing the velocity u_i of a fluid with uniform density ρ and kinematic viscosity ν:

$$\rho \partial_t u_i + \rho u_j \partial_j u_i = \rho \nu \partial_{jj} u_i - \partial_i p + \zeta u_i + f_i \tag{1}$$

where p is pressure, ζ is constant energy injection forcing applied to modes with wavenumber $\kappa < 4\pi/L$ [12], $f_i = -c\partial_i \phi$ is the force of the interface on the fluid, and indices $i, j \in \{1,2,3\}$ denote vector components with repeated indices summed. Incompressibility is enforced by:

$$\partial_i u_i = 0, \tag{2}$$

and we simulate two immiscible phases by coupling to the Cahn–Hilliard equations for a scalar field $-1 < c < 1$ [13]:

$$\partial_t c + u_j \partial_j c = m \partial_{ii} \phi. \tag{3}$$

Here, $c = 1$ corresponds to the dispersed phase (drop) and $c = -1$ to the carrier phase. The mobility m controls the relaxation time of the fluid-fluid interface. We model immiscibility between components through the chemical potential:

$$\phi = \beta(c^2 - 1)c - \alpha \partial_{ii} c, \tag{4}$$

where α and β are model parameters determining the interface thickness $w = 4\sqrt{2\alpha/\beta}$ and surface tension σ. As interface thickness vanishes ($w \to 0$), $\sigma \to \frac{1}{3}\sqrt{8\alpha\beta}$ [14]. We express the interface thickness and relaxation time via two dimensionless numbers: the Cahn number $\mathrm{Cn} = d^{-1}\sqrt{\alpha/\beta}$ and Peclet number $\mathrm{Pe} = u'd^2/(m\sqrt{\alpha\beta})$, where d is drop diameter and u' is the root mean square fluid velocity. Following Magaletti et al. [14], we choose the optimal balance $\mathrm{Pe} = \frac{1}{3}\mathrm{Cn}^{-1}$ minimizing both interface thickness and relaxation time. The reader can find further details on our numerical method for solving the Cahn–Hilliard Navier–Stokes equations in Vela-Martín and Avila [15].

Equations 1–3 are solved on a graphical processing unit (GPU) using a pseudospectral method with 256^3 grid points. A de-aliasing procedure is employed to remove spurious interactions of discretised nonlinear terms, retaining only $(256 \times 2/3)^3$ modes when projecting into Fourier space, so that the maximum resolved wavenumber is $K = 2\pi M/(3L)$. We maintain the flow in a statistically stationary state by adjusting the forcing coefficient ζ such that the total kinetic energy injected per unit time ε is constant. We choose the constant to ensure adequate numerical resolution, quantified by $K\eta = 4$, where $\eta = (\nu^3/\varepsilon)^{1/4} = 0.00746L$ is the Kolmogorov length scale.

We conducted hundreds of independent, time-resolved simulations, each starting with a single initially spherical drop that is tracked until breakup. The simulations cover a range of Weber numbers to explore the influence of inertial-to-capillary forces on drop deformation.

$$\mathrm{We} = \frac{\rho u_d^2 d}{\sigma}, \tag{5}$$

where $u_d = \varepsilon^{1/3} d^{1/3}$ is the turbulent velocity at the scale of the drop diameter. The dissipation rate is $\varepsilon = \nu\langle \partial_j u_i \partial_j u_i \rangle$, and we define the velocity $u_d = \varepsilon^{1/3} d^{1/3}$ and timescale $t_d = d/u_d$ of the eddy at the drop diameter d, à la Kolmogorov [1]. Table 1 shows the Weber number with the number of simulations analysed. As explained in section 4, we only analysed cases in which the simulation continued for more than $5t_d$ without breaking; in the highest We case, we initialised 599 drops, and only 7 survived for more than $5t_d$. Note that in these proceedings, we use $\mathrm{We} = \infty$ to denote the single-phase case.

The turbulence has a Taylor Reynolds number $\mathrm{Re}_\lambda = 58$, defined as $\mathrm{Re}_\lambda = u'\lambda/\nu$, where u' is the root-mean-square velocity fluctuation, λ the Taylor microscale, and ν the kinematic viscosity. Plotted data and post-processing routines for this spectral analysis are available online [16].

4 RESULTS

Figure 1 shows snapshots of the interface at each Weber number in our study. In the high Weber number cases, turbulent inertial forces dominate over surface tension; fluid motion stretches the interface, and the drops tend to elongate into filaments [5]. The low We drop remains almost spherical, as surface tension is strong enough to resist deformation.

To understand the temporal and spatial scales characterising drop-turbulence interaction, we compute both wavenumber and frequency spectra of the turbulent velocity field. Following Clark Di Leoni et al. [17], we use the hat to represent

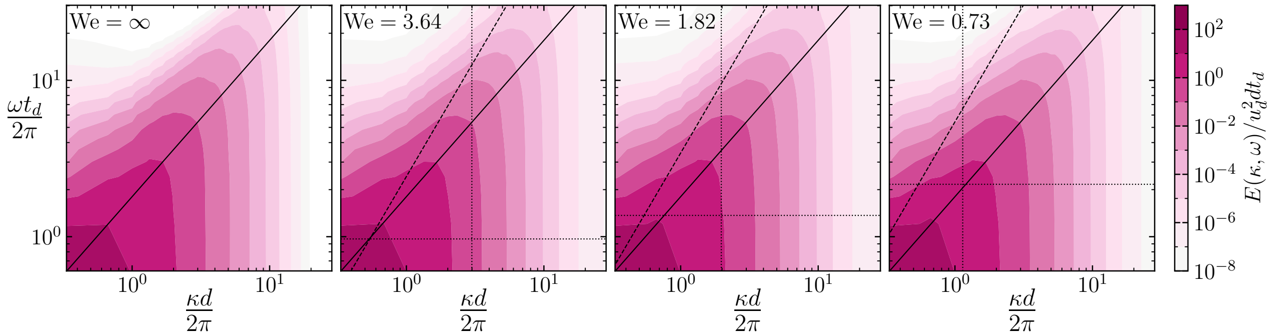

Figure 2. Turbulent kinetic energy spectra. The solid line is the advection speed $\omega = u'\kappa$, the dashed line is the capillary wave speed $\omega^2 = \sigma\rho^{-1}\kappa^3$. Vertical and horizontal dotted lines show the wavenumber $2\pi/d_H$ of the Hinze scale, and the capillary frequency $2\pi/t_\sigma$.

the four-dimensional Fourier transform of a general field s:

$$\hat{s}(\boldsymbol{\kappa},\omega) = \int_{t_d}^{4t_d}\int_0^L\int_0^L\int_0^L H(t)\, s(\boldsymbol{x},t) \exp(\mathrm{i}\kappa_j x_j - \mathrm{i}\omega t)\, \mathrm{d}^3x\, \mathrm{d}t \qquad (6)$$

where $\boldsymbol{\kappa}$ is the wavevector, non-italic $\mathrm{i} = \sqrt{-1}$ is the imaginary unit and the Hann window:

$$H(t) = \sin^2 \frac{\pi(t-t_d)}{3t_d} \qquad (7)$$

enforces periodicity over the record length $t_d \le t < 4t_d$, where $t_d = d/u_d$ is the eddy turnover time at the scale of the drop. We have excluded the initial t_d and final t_d from each time-series to remove transient effects that occur during equilibration and breakup [9]. The spatio-temporal turbulent kinetic energy spectrum follows by multiplying the velocity field $\hat{u}_i$ with its complex conjugate $\hat{u}_i^*$, and, using the isotropic nature of our setup, we integrate over spherical shells in κ-space:

$$E(\kappa,\omega) = \left\langle \iiint \tfrac{1}{2}\hat{u}_i(\boldsymbol{\kappa},\omega)\hat{u}_i^*(\boldsymbol{\kappa},\omega)\delta(\kappa_j\kappa_j - \kappa^2)\,\mathrm{d}^3\kappa \right\rangle_N. \qquad (8)$$

where angled brackets represent an average over the ensemble N of drops that did not break before $t = 5t_d$. Density is constant in our system, so we have omitted it here. Of course, integrating over all components and multiplying by density gives the mean kinetic energy per unit volume in the fluid:

$$\rho \iint E(\kappa,\omega)\mathrm{d}\kappa\mathrm{d}\omega = \tfrac{1}{2}\rho u'^2 \qquad (9)$$

We show the turbulent kinetic energy spectra in figure 2. We see that, at all Weber numbers, kinetic energy is concentrated at the large length scales and time scales. There is a ridge in $E(\kappa,\omega)$ near the advection speed $\omega = u'\kappa$ due to the large-scale motion, but with a slightly higher frequency. A reflection symmetry in this line would indicate that Taylor's frozen flow hypothesis [18] holds. The plot is not quite symmetric in this line, likely due to the multiscale nature of the eddies, which advect one another in the flow. The drop produces a slight increase in energy at short timescales and length scales in the flow.

We can quantify the interaction between the droplet interface and the surrounding fluid via the real part of the spectral work rate associated with the interfacial forcing (f_i):

$$F(\kappa,\omega) = \left\langle \iiint \Re!\left[\hat{u}_i^*(\boldsymbol{\kappa},\omega), \hat{f}_i(\boldsymbol{\kappa},\omega)\right] \delta!\left(\kappa_j\kappa_j - \kappa^2\right), \mathrm{d}^3\kappa \right\rangle_N. \qquad (10)$$

These results are shown in figure 3. They provide a direct interpretation of the droplet-induced modulation of ($E(\kappa,\omega)$): at large spatial scales and long temporal scales, (F) is negative, indicating net energy transfer from the flow to the droplet interface, whereas at smaller scales and higher frequencies, (F) becomes positive, corresponding to energy injection from the droplet into the flow.

Next, we derive an expression for the spatio-temporal spectrum of the interfacial energy. The interfacial energy part of the Cahn–Hilliard free energy functional is [14]

$$\mathscr{F}[\phi] = \int_0^L\int_0^L\int_0^L \frac{Cn}{2}\partial_i\phi\partial_i\phi\mathrm{d}^3x. \qquad (11)$$

In Fourier space, this becomes:

$$\mathscr{F}[\hat{\phi}] = \iiint \frac{Cn}{2}\kappa_i\kappa_i\hat{\phi}\hat{\phi}^*\mathrm{d}^3\kappa. \qquad (12)$$

In the limit of a sharp interface, $\mathscr{F}[\phi] \to \sigma A$, where A is the interface area. In our case, the surface tension σ is constant in space, so the interfacial energy and area spectra are simply related by a factor of σ. Hence, we define the interface-area spectrum:

$$A(\kappa,\omega) = \left\langle \iiint \kappa_i\kappa_i\,\hat{\phi}(\boldsymbol{\kappa},\omega)\,\hat{\phi}^*(\boldsymbol{\kappa},\omega)\,\delta(\kappa_j\kappa_j - \kappa^2)\,\mathrm{d}^3\kappa \right\rangle_N. \qquad (13)$$

Analogously with the turbulent kinetic energy spectrum in (9), the sum of all modes is the total drop area:

$$\iint A(\kappa,\omega)\,\mathrm{d}\kappa\,\mathrm{d}\omega = A. \qquad (14)$$

We plot this in figure 4. We see that the interface holds energy at low frequencies, with a peak at the diameter lengthscale. Compared to the turbulent kinetic energy spectrum, a larger fraction of the energy is stored at short length scales.

The one-dimensional wavenumber spectrum follows from integrating the spatio-temporal spectrum over all frequencies:

$$E(\kappa) = \int E(\kappa,\omega)\,\mathrm{d}\omega, \qquad (15)$$

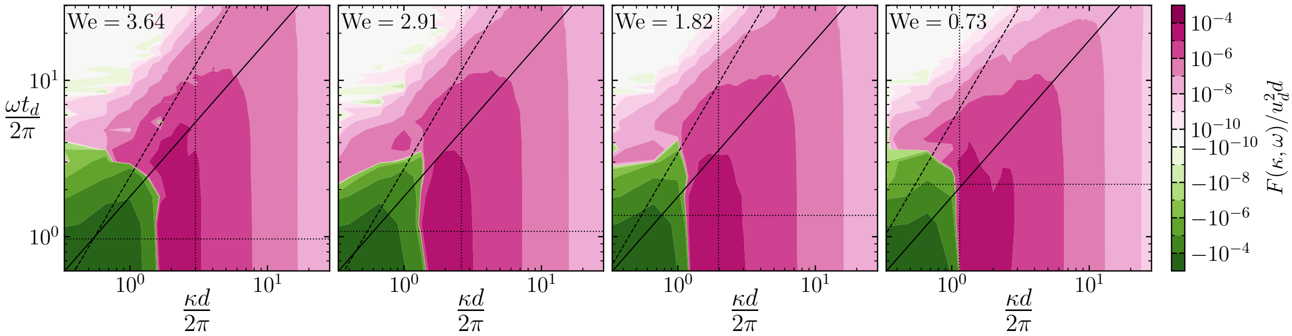

Figure 3. Power spectra of the interfacial force on the fluid. The solid line is the advection speed $\omega = u'\kappa$, the dashed line is the capillary wave speed $\omega^2 = \sigma\rho^{-1}\kappa^3$. Vertical and horizontal dotted lines show the wavenumber $2\pi/d_H$ of the Hinze scale, and the capillary frequency $2\pi/t_\sigma$.

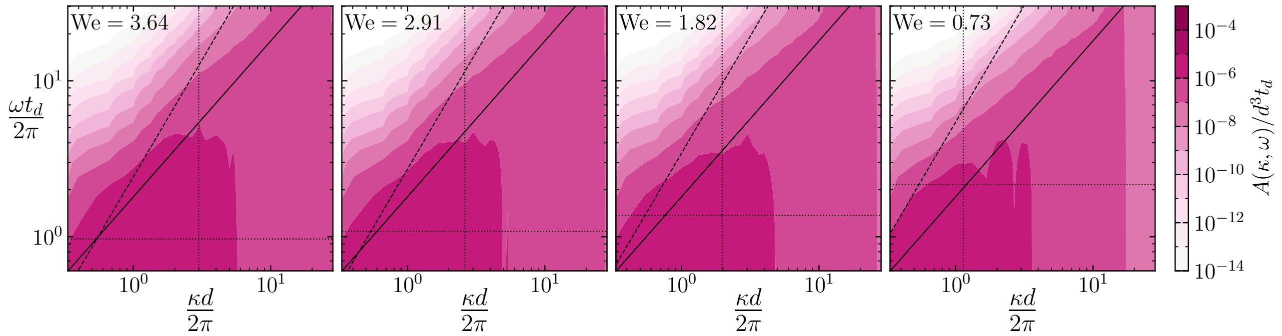

Figure 4. Spectra of the drop interfacial area. The solid line is the advection speed $\omega = u'\kappa$, the dashed line is the capillary wave speed $\omega^2 = \sigma\rho^{-1}\kappa^3$. Vertical and horizontal dotted lines show the wavenumber $2\pi/d_H$ of the Hinze scale, and the capillary frequency $2\pi/t_\sigma$.

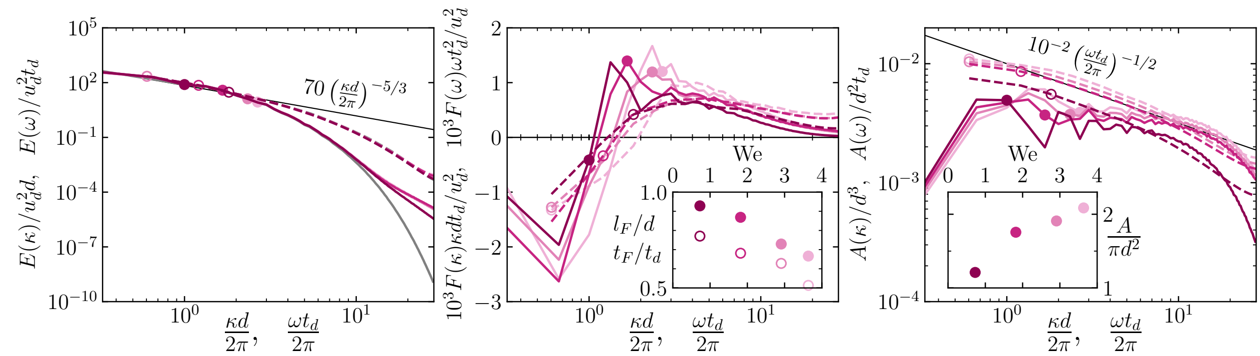

Figure 5. Spatial and temporal spectra of fluid kinetic energy (left panel), coupling to the interface (middle panel), and interfacial area (right panel). Left panel: Energy spectra in wavenumber space $E(\kappa)$ (solid lines) and frequency space $E(\omega)$ (dashed lines), with the black line showing Kolmogorov's $\kappa^{-5/3}$ scaling. Middle panel: Spectral distribution of the work done by the surface tension force, $F(\kappa)$ (solid lines) and $F(\omega)$ (dotted lines), multiplied by wavenumber κ and frequency ω respectively. The inset shows the crossover length scale l_F (filled circles) and time scale t_F (empty circles), at which $F = 0$. Right panel: the interfacial areas $A(\kappa)$ (solid lines) and $A(\omega)$ (dotted lines). The inset shows the mean drop area divided by its unperturbed area, πd^2. We make all variables dimensionless using the velocity u_d, turnover time t_d, and drop diameter d. We mark the spectra with filled circles at the wavenumber $2\pi/d_H$ of the Hinze scale, and open circles at the capillary frequency $2\pi/t_\sigma$.

Similarly, the one-dimensional frequency spectrum is:

$$E(\omega) = \int E(\kappa,\omega)\,\mathrm{d}\kappa, \tag{16}$$

and analogous one-dimensional spectra $F(\kappa)$, $F(\omega)$, $A(\kappa)$, and $A(\omega)$ are obtained in the same way.

The left panel of figure 5 displays the energy spectra. The wavenumber spectrum closely follows Kolmogorov inertial-range scaling [1],

$$E(\kappa) = 70 d u_d^2 \left(\frac{\kappa d}{2\pi}\right)^{-5/3}, \tag{17}$$

over nearly a decade before viscous dissipation dominates at small scales. The large prefactor results from our choice to normalise with a characteristic velocity u_d, which is smaller than the root-mean-square velocity u'. Compared to the single-phase flow, the presence of a drop leads to a modest increase in energy at small scales, and surprisingly, the effect is most pronounced in the high Weber number case: the surface tension force is weaker, but the area is greater. This suggests that as We $\to \infty$, the energy spectrum may not tend to the single-phase turbulent energy spectrum. The frequency spectrum $E(\omega)$ closely collapses onto the wavenumber spectrum when frequencies are scaled by the turnover time t_d of eddies with the same size as the drop. However, appreciable energy persists at higher frequencies. We attribute this to the fact that the viscous Laplacian operator imposes strict exponential decay in wavenumber space but does not enforce temporal continuity of the velocity field.

The middle panel of figure 5 shows how the drop exchanges energy with the turbulent flow. Both wavenumber and frequency spectra show that drops absorb energy from large, low-frequency eddies (negative F at low κ and ω) and return energy to small, high-frequency eddies (positive F at high κ and ω). The crossover occurs at a similar length scale to the drop diameter d and a similar timescale to the inertial time t_d. This sign change with wavenumber has been observed in flows containing drops [19], and particles [20, 2]; indeed, as the Weber number increases, the length and timescales of the crossover become smaller. As We $\to 0$, the drop tends to spherical, the length scale of the crossover tends to d and the timescale tends to t_d. Interestingly, the power input by the drop on the fluid tends to zero at short length scales, but converges on a finite value for short timescales. The peak rate of energy extraction from the flow is

$$10^3 F(\kappa)\kappa d t_d / u_d^2 = -2.63 \tag{18}$$

at $\kappa d/2\pi = 2/3$. Hence, the timescale of removal of kinetic energy is

$$E/F = 70(2/3)^{-5/3} t_d / 2.63 \times 10^{-3} = 5.2 \times 10^4 t_d. \tag{19}$$

In other words, the drop is having an almost negligible effect on the fluid kinetic energy at these large scales, which explains the negligible changes in the energy spectrum $E(\kappa)$ at the large scales when drops are added.

The right panel of figure 5 shows the interfacial-area spectra of the drops. Both the spatial and temporal spectra exhibit an increase in interfacial area with increasing Weber number. In the limit We $\to 0$, the total area,

$$A = \int A(\kappa)\,\mathrm{d}\kappa = \int A(\omega)\,\mathrm{d}\omega \tag{20}$$

approaches that of an undeformed drop πd^2. The temporal spectra $A(\omega)$ show that the majority of energy is contained in the slow oscillations; indeed, the spectrum decays similarly to $A \sim \omega^{-1/2}$ for the majority of the frequencies measured. The spatial spectrum, on the other hand, shows that reducing the Weber number causes the interface to lose energy at the small length scales and gain energy at the large scales. This is because increasing surface tension makes the interface smoother, eliminating small-scale perturbations. The drop-off in energy for $\kappa d/2\pi > 10$ is a numerical artefact due to the finite thickness of the interface in the Cahn–Hilliard equation.

5 CONCLUSIONS

We have presented the first spatio-temporal energy spectra of drops in homogeneous isotropic turbulence, computed from an ensemble of hundreds of direct numerical simulations of the Cahn–Hilliard–Navier–Stokes equations across four Weber numbers. Analysing the drops during their stage of dynamic equilibrium with the surrounding flow, we find three principal results.

1. The turbulent kinetic energy spectrum $E(\kappa,\omega)$ closely follows Kolmogorov inertial-range scaling at all Weber numbers, with drops inducing a modest increase in energy at small scales and short timescales. The magnitude of this increase grows with Weber number, suggesting that the energy spectrum does not tend to its single-phase counterpart even in the limit We $\to \infty$.
2. The spatio-temporal spectrum of the interfacial force on the fluid, $F(\kappa,\omega)$, confirms that drops act as a spectral shortcut in frequency and length: they absorb kinetic energy from large, slow eddies and return it to small, fast eddies, with a crossover near the drop diameter d and inertial timescale t_d. As We $\to 0$, this crossover converges towards the behaviour of a rigid sphere, consistent with earlier particle-laden results [2].
3. The interfacial area spectrum $A(\kappa,\omega)$ is dominated by slow, large-scale deformations, with its spatial peak at the drop diameter lengthscale. A clear ridge appears in $E(\kappa,\omega)$, $F(\kappa,\omega)$, and $A(\kappa,\omega)$ near the advective scaling $\omega = u'\kappa$, consistent with large-scale interfacial structures being transported by the surrounding turbulent flow.

Future work should extend this analysis to larger density contrasts, such as water drops in air [21], where the backreaction of the drop on the turbulent flow is expected to be considerably stronger, and to higher Reynolds numbers to better separate the inertial and capillary wave speeds in the spatio-temporal plane.

6 KEYWORDS

Drop deformation; turbulence; Weber number; direct numerical simulation; phase-field method; spatio-temporal spectrum.

REFERENCES

[1] A. N. Kolmogorov. “The Local Structure of Turbulence in Incompressible Viscous Fluid for Very Large Reynolds Numbers”. In: *Proc. R. Soc. Lond. A. Math. Phys. Sci.* 434 (1890, 1941), pp. 9–13. JSTOR: 51980. URL: http://www.jstor.org/stable/51980.

[2] I. Cannon, S. Olivieri, and M. E. Rosti. “Spheres and Fibers in Turbulent Flows at Various Reynolds Numbers”. In: *Phys. Rev. Fluids* 9.6 (2024), p. 064301. DOI: 10.1103/PhysRevFluids.9.064301.

[3] P. Perlekar, D. Mitra, and R. Pandit. “Direct Numerical Simulations of Statistically Steady, Homogeneous, Isotropic Fluid Turbulence with Polymer Additives”. In: *Phys. Rev. E* 82.6 (2010), p. 066313. ISSN: 1539-3755, 1550-2376. DOI: 10.1103/PhysRevE.82.066313.

[4] M. Crialesi-Esposito, S. Chibbaro, and L. Brandt. “The Interaction of Droplet Dynamics and Turbulence Cascade”. In: *Commun Phys* 6.1 (1 2023), pp. 1–8. ISSN: 2399-3650. DOI: 10.1038/s42005-022-01122-8.

[5] I. Cannon, G. Soligo, and M. E. Rosti. “Morphology of Clean and Surfactant-Laden Droplets in Homogeneous Isotropic Turbulence”. In: *J. Fluid Mech.* 987 (2024), A31. ISSN: 0022-1120, 1469-7645. DOI: 10.1017/jfm.2024.380.

[6] D. Maestrini, G. Dematteis, A. Benetazzo, and M. Onorato. “Revealing Wave-Wave Resonant Interactions in Ocean Wind Waves”. In: *Commun Phys* (2026). ISSN: 2399-3650. DOI: 10.1038/s42005-026-02653-0.

[7] M. Ayala, M. P. Encinar, C. Meneveau, and D. F. Gayme. “Spatio-Temporal Model of Turbulence over Waves”. In: *J. Phys.: Conf. Ser.* 3230.1 (2026), p. 012025. ISSN: 1742-6596. DOI: 10.1088/1742-6596/3230/1/012025.

[8] G. Foggi Rota, R. K. Singh, A. Chiarini, C. Amor, G. Soligo, D. Mitra, and M. E. Rosti. “The Broken Link between Space and Time in Elastic Turbulence”. In: *Int. J. Multiph. Flow* 197 (2026), p. 105630. ISSN: 0301-9322. DOI: 10.1016/j.ijmultiphaseflow.2026.105630.

[9] I. Cannon, D. Morón, A. Vela-Martín, and M. Avila. “Strain-Driven Drop Breakup in Turbulence”. In: *J. Phys.: Conf. Ser.* 3230.1 (2026), p. 012006. ISSN: 1742-6596. DOI: 10.1088/1742-6596/3230/1/012006.

[10] U. E. Paulista, P. D. E. P.-g. Em, and C. Biológicas. *Computational Methods for Multiphase Flow*. Ed. by A. Prosperetti and G. Tryggvason. Cambridge: Cambridge University Press, 2007. ISBN: 978-0-511-60748-6. URL: http://ebooks.cambridge.org/ref/id/CBO9780511607486.

[11] S. O. Unverdi and G. Tryggvason. “A Front-Tracking Method for Viscous, Incompressible, Multi-Fluid Flows”. In: *J. Comp. Phys.* 100.1 (1992), pp. 25–37. ISSN: 0021-9991. DOI: 10.1016/0021-9991(92)90307-K.

[12] J. Jiménez, A. A. Wray, P. G. Saffman, and R. S. Rogallo. “The Structure of Intense Vorticity in Isotropic Turbulence”. In: *J. Fluid Mech.* 255 (1993), pp. 65–90. ISSN: 1469-7645, 0022-1120. DOI: 10.1017/S0022112093002393.

[13] D. Jacqmin. “Calculation of Two-Phase Navier–Stokes Flows Using Phase-Field Modeling”. In: *J. Comp. Phys.* 155.1 (1999), pp. 96–127. ISSN: 00219991. DOI: 10.1006/jcph.1999.6332.

[14] F. Magaletti, F. Picano, M. Chinappi, L. Marino, and C. M. Casciola. “The Sharp-Interface Limit of the Cahn–Hilliard/Navier–Stokes Model for Binary Fluids”. In: *J. Fluid Mech.* 714 (2013), pp. 95–126. ISSN: 0022-1120, 1469-7645. DOI: 10.1017/jfm.2012.461.

[15] A. Vela-Martín and M. Avila. “Deformation of Drops by Outer Eddies in Turbulence”. In: *J. Fluid Mech.* 929 (2021), A38. ISSN: 0022-1120, 1469-7645. DOI: 10.1017/jfm.2021.879.

[16] I. Cannon. *strainBox*. 2025. URL: https://gitlab.zarm.uni-bremen.de/ianto-cannon/strainbox.

[17] P. Clark Di Leoni, P. J. Cobelli, and P. D. Mininni. “The Spatio-Temporal Spectrum of Turbulent Flows”. In: *Eur. Phys. J. E* 38.12 (2015), p. 136. ISSN: 1292-8941, 1292-895X. DOI: 10.1140/epje/i2015-15136-x.

[18] G. I. Taylor. “The Spectrum of Turbulence”. In: *Proc. A* 164.919 (1938), pp. 476–490. ISSN: 0080-4630. DOI: 10.1098/rspa.1938.0032.

[19] M. Crialesi-Esposito, M. E. Rosti, S. Chibbaro, and L. Brandt. “Modulation of Homogeneous and Isotropic Turbulence in Emulsions”. In: *J. Fluid Mech.* 940 (2022), A19. ISSN: 0022-1120, 1469-7645. DOI: 10.1017/jfm.2022.179.

[20] A. Chiarini and M. E. Rosti. “Finite-Size Inertial Spherical Particles in Turbulence”. In: *J. Fluid Mech.* 988 (2024), A17. ISSN: 0022-1120, 1469-7645. DOI: 10.1017/jfm.2024.421.

[21] R. Ni. “Deformation and Breakup of Bubbles and Drops in Turbulence”. In: *Annu. Rev. Fluid Mech.* 56 (Volume 56, 2024 2024), pp. 319–347. ISSN: 0066-4189, 1545-4479. DOI: 10.1146/annurev-fluid-121021-034541.